HHS Public Access

Author manuscript

Biomaterials. Author manuscript; available in PMC 2022 January 01.

Published in final edited form as:

Biomaterials. 2021 January ; 265: 120401. doi:10.1016/j.biomaterials.2020.120401.

Self-assembling Multidomain Peptide Hydrogels accelerate Peripheral Nerve Regeneration after Crush Injury

Tania L. Lopez-Silva[*,a], **Carlo D. Cristobal**[*,b,d], **Cheuk Sun Edwin Lai**[a], **Viridiana Leyva-Aranda**[a], **Hyun Kyoung Lee**[#,b,c,d], **Jeffrey D. Hartgerink**[#,a]

[a]Department of Chemistry and Bioengineering, Rice University, Houston, Texas 77005, USA

[b]Integrative Program in Molecular and Biomedical Sciences, Baylor College of Medicine, Houston, Texas 77030, USA

[c]Department of Pediatrics-Neurology, Baylor College of Medicine, Houston, Texas 77030, USA

[d]Jan and Dan Duncan Neurological Research Institute, Texas Children's Hospital, Houston, Texas 77030, USA

Abstract

Multidomain peptide (MDP) hydrogels are a class of self-assembling materials that have been shown to elicit beneficial responses for soft tissue regeneration. However, their capacity to promote nervous system regeneration remains unknown. The peripheral nervous system (PNS) substantially recovers after injury, partly due to the abundance of extracellular matrix (ECM) components in its basal lamina. However, severe peripheral nerve injuries that significantly damage the ECM continue to be a major clinical challenge as they occur at a high rate and can be extremely detrimental to patients' quality of life. In this study, a panel of eight MDPs were designed to contain various motifs mimicking extracellular matrix components and growth factors and successfully self-assembled into injectable, nanofibrous hydrogels. Using an in vitro screening system, various lysine based MDPs were found to enhance neurite outgrowth. To test their capacity to promote nerve regeneration *in vivo*, rat sciatic nerve crush injury was performed with MDP hydrogels injected directly into the injury sites. MDP hydrogels were found to enhance macrophage recruitment to the injury site and degrade efficiently over time. Rats that were injected with the MDP hydrogel K_2 and laminin motif-containing MDPs K_2-IIKDI and K_2-IKVAV were

[#]**Corresponding Authors:** hyunkyol@bcm.edu, jdh@rice.edu.
[*]TLLS and CDC contributed equally

Author Contributions

TLLS, CDC, HKL, and JDH designed the project, created experimental design, and wrote the manuscript. Confocal microscopy and data analysis with IMARIS were performed in the Neurovisualization core of the BCM/NRI IDDRC. TLLS, EL and VLA prepared peptide materials. TLLS and EL characterized peptides. TLLS and CDC conducted in vitro, in vivo studies, and analyzed data. TLLS, CDC, HKL and JDH interpreted the data.

Appendix A. Supplementary data

Supplementary data related to this article can be found at https://doi. org/10.1016/j.biomaterials.2020.120401.

Data Availability Statement

The raw/processed data required to reproduce these findings cannot be shared at this time due to technical or time limitations.

found to have significantly accelerated functional recovery and remyelination compared to those injected with HBSS or other MDPs. These results demonstrate that MDPs enhance neurite outgrowth and promote a multicellular pro-regenerative response in peripheral nerve injury. This study provides important insights into the potential of MDPs as biomaterials for nerve regeneration and other clinical applications.

Keywords

Peptide hydrogel; Peripheral Nerve Regeneration; Sciatic nerve crush injury; bioactive materials; peptide mimics

1. Introduction

Peptide-based materials have shown great promise for biomedical applications because of their capacity to mimic the structure and complexity of the extracellular matrix (ECM), which is usually damaged or lost in injury and disease [1]. These materials can be designed to form hydrogels - crosslinked fibrous networks with high water content - that provide physical similarity to tissues [2]. Furthermore, hydrogels can be designed to be fully composed of natural amino acids, providing inherent biocompatibility, structural diversity, tunable mechanical properties, degradation without adverse effects, and a platform for the incorporation of bioactive cues [3–8]. In this category are the self-assembling multidomain peptide (MDP) hydrogels, which rely on the molecular assembly of amphiphilic peptides into nanofibers. MDPs are composed of a core of alternating hydrophilic and hydrophobic residues which drive assembly and flanking domains which mediate or control assembly. In aqueous solutions, the amphiphilic core drives aggregation by hydrophobic packing and hydrogen bonding along the peptide backbone, while the N- and C-terminal domains controls self-assembly with ion-ion repulsion or steric constraints [9]. The most common MDP design utilizes ionic residues such as lysine, arginine or glutamate to modulate molecular assembly and hydrogel formation in response to pH changes or addition of multivalent ions [5,9,10]. However, non-ionic neutral MDP hydrogels are also formed when steric interactions are used to regulate self-assembly and hydrogelation of these peptides [11]. The MDP family provides a diversity of scaffolds that can be designed or used for different bioactivity or specific applications, such as small-molecule and protein delivery, cell support, or tissue engineering [12–16].

Previous work with the lysine-based MDP, $K_2(SL)_6K_2$ (herein referred as K_2), demonstrated that this injectable material evokes favorable host responses, which are beneficial for wound healing and tissue regeneration [16–18]. When implanted subcutaneously in an animal model, the hydrogel is rapidly infiltrated by immune cells and elicits acute inflammation that resolves over time. This inflammatory response is characterized by the presence of macrophages, which remodel the material and secrete growth factors, such as vascular endothelial growth factor (VEGF) and nerve growth factor (β-NGF). As a result, the K_2 MDP hydrogel induces blood vessel formation within the implant and surrounding tissue [17]. These observations demonstrate the potential of K_2 hydrogel as a biomaterial for promoting soft tissue regeneration. In particular, we are interested in evaluating the

capability of K_2 MDP to enhance nerve regeneration in the peripheral nervous system (PNS). Injuries in the PNS occur at a high frequency, and despite its robust regenerative capacity, severe peripheral nerve injuries still lead to sensory or motor deficits affecting overall quality of life [19]. The ECM components that comprise the basal lamina are known to be crucial for the regenerative response [20]; thus, materials that mimic healthy ECM have emerged as potentially powerful strategies to improve clinical outcomes after injury [1].

The regenerative response after injury to the PNS occurs in discrete stages and requires the orchestrated activity of multiple cell types. After a major injury event, such as nerve crush or neurotmesis (complete severing of the nerve), the distal portion of the peripheral nerve undergoes a process called Wallerian degeneration. Initially, detached axon segments undergo catastrophic disintegration of the cytoskeleton into cellular debris [21,22]. Soon after, Schwann cells start their dedifferentiation, degrading their own myelin and phagocytosing extracellular debris [23–25]. These Schwann cells secrete cytokines and chemokines, recruiting immune cells like macrophages and monocytes into the injury site, which assume a primary role in debris removal and growth factor production [26,27]. During this phase, Schwann cells proliferate and secrete ECM molecules and trophic factors which promote axon regeneration [27,28]. This process, along with the presence of an ECM basal lamina, creates a permissive environment for axonal outgrowth from the proximal side of the injury, reinnervation, and remyelination [29]. Owing to the complexity of this process, strategies for promoting peripheral nerve regeneration must promote favorable responses from multiple cell types, which can then result in overall recovery.

We have previously determined that K_2 elicits many of the factors required for peripheral nerve regeneration, including macrophage infiltration, cell proliferation, and production of neurotrophic factors, highlighting its potential bioactivity in this context. Furthermore, the high-water content, nanofibrous structure, and biocompatibility of MDP hydrogels make them promising materials to mimic healthy ECM, promoting recovery. Using this rationale, we utilized K_2 as a base peptide scaffold, which by itself would elicit favorable responses, and incorporated bioactive peptide motifs which we hypothesized would elicit additional favorable responses with PNS cells. In this work we evaluated the regenerative properties of K_2 and K_2-based peptide hydrogels with additional motifs incorporated into the peptide sequence (Figure 1 and Table 1). The peptide motifs are derived from ECM proteins and growth factors and were found to mimic their bioactivity by enhancing neurite outgrowth, facilitating cell adhesion and material degradation [30–37]. For instance, the peptide motifs RNIAEIIKDI, IKVAV, IIKDI, and KDI are derived from Laminin, a major component of the surrounding nerves which has an active role in glial cell support [30]. The short peptide sequence VFDNFVLK mimics the activity of Tenascin C, a protein that has a key role in nerve development and regeneration [35,36,38,39]. We hypothesize that these functionalized peptides will improve nerve regeneration and provide an additional beneficial effect over the favorable inflammatory response provoked by the K_2 base sequence (Figure 1). As for comparisons, we utilized Matrigel, a commonly used animal-derived ECM matrix [40–42], and a non-ionic MDP ($Hyp_5(SL)_6Hyp_5$, herein called O_5), which is not known to elicit pro-inflammatory responses [11]. The goal of this project is to find the peptide hydrogel that most effectively accelerates the regeneration of sciatic nerve after a crush injury. To

accomplish this, first we performed an *in vitro* screening method to test the neurite-promoting activity of each peptide, followed by MDP administration in a rat sciatic nerve crush injury model to test the most promising materials from the initial screen. This study will provide important insight into the potential of MDPs as biomaterials for nerve regeneration and lead to the development of better biomaterials for clinical applications.

2. Materials and Methods

2.1. Material preparation and characterization

2.1.1. Peptide synthesis—All peptides (Table 1 and Table S1) were synthesized using a standard FMOC based solid-phase peptide synthesis. Detailed experimental method is available in the supporting information. Peptides were dialyzed against deionized Milli-Q water for 4–5 days in 100–500 Da MWCO dialysis tubing (Spectra/Por, Spectrum Laboratories Inc. Rancho Dominguez, CA), and pH-adjusted to 7–7.4. Peptide solutions were sterile filtered with a 0.2 μm polystyrene filter, frozen, lyophilized, and stored at −20°C. Peptide mass was confirmed by mass spectroscopy using an Autoflex MALDI-TOF MS (Figure S1) (Bruker Instruments, Billerica, MA).

2.1.2. Secondary structure characterization

2.1.2.1. Circular Dichroism (CD) Spectroscopy: Peptide solutions of 0.1% for K_2-KDI and K_2-TenC, and 1% for K_2-IKVAV were prepared in 149 mM sucrose: 0.5X Hank's Balanced Salt Solution. For K_2-IIKDI a 2% by weight solution was prepared in 298 mM sucrose solution. CD spectra acquisition was performed in a CD Jasco J-810 spectropolarimeter (Jasco, Inc. Easton, MD) using a 0.1 and 0.01 cm quartz cuvette. Data were collected at room temperature from 180 to 250 nm at a speed of 50 nm/min and a 0.1 nm data pitch. The final CD spectra is an average of five scans.

2.1.2.2. Attenuated Total Reflectance Fourier Transform Infrared (ATR-FTIR) Spectroscopy: Peptide samples used for CD spectroscopy were dried under nitrogen flow on a golden gate diamond window of an ATR stage. IR spectra were collected using a Jasco FT/IR-660 plus spectrometer (Jasco Inc., Easton, MD) at a 1 cm^{-1} resolution with an accumulation of 32 scans. The background was subtracted from the resulting spectra.

2.1.3. Peptide hydrogelation—Peptides were dissolved in 298 mM sucrose solution in Milli-Q water to obtain a 2% by weight (20 mg/mL) concentration. Peptide solutions were then diluted to 1% by weight with 1X Hank's Balanced Salt Solution (HBSS) to induce hydrogelation. The final concentration for most of the peptides was 10 mg/mL peptide in 149 mM sucrose and 0.5X HBSS, except for K_2-IIKDI, which only forms a hydrogel at 2% by weight in 298 mM sucrose solution. In the case of O_5, the 1% by weight peptide solution in 149mM sucrose:0.5X HBSS was ultrasonicated with a 2 mm microprobe with 10 pulses and 1 min relaxation time as described in previous work. [11] Matrigel (Corning, Bedford MA) was allowed to thaw on ice prior to injection and gelation occurred in situ as recommended by Corning protocols.

2.1.4. Scanning Electron Microscopy (SEM)—Peptide hydrogels were dehydrated with a series of ethanol treatments (30% to 100%). Ethanol was removed by critical point drying using an EMS 850 critical point dryer (Electron Microscopy Sciences, Hatfield, PA). Samples were mounted onto SEM pucks using a conductive carbon tape, coated with 4–5 nm of gold using a Denton desk V Sputter system (Denton Vacuum, Moorestown, NJ). Samples were analyzed using a JEOL 6500 Scanning Electron Microscope (JEOL Inc., Peabody, MA).

2.1.5. Oscillatory Rheology—Viscoelastic properties of peptide hydrogels were analyzed by an AR-G2 rheometer (TA Instruments, New Castle, DE). Peptide was prepared 24 hours before the test. 150 μL of each peptide hydrogel was analyzed using a 12 mm stainless-steel parallel plate set to a 1000 μm gap height. Strain sweep test was performed from 0.01 to 200% strain at a 1 rad/s frequency. Shear recovery was analyzed by monitoring the storage (G') and loss (G") moduli at 1% strain for 10 min after treatment with 200% strain for 1 min (Figure S2).

2.2. Screening of bioactive peptides by 2D primary neuron culture

2.2.1. Peptide coating of cover glasses—Peptide solutions or Poly-D-Lysine (Millipore Sigma) of 100 μg/mL were prepared in sterile ultrapure water. The surface of 12 mm circular cover glasses was coated with the peptide solution and left overnight at 4°C. Excess peptide solution was aspirated, and coverslips were air-dried before cell culture. Peptide coating was performed following a blinding procedure as described in supporting information.

2.2.2. Primary neuronal culture—Primary neuronal cultures were performed as previously described [44]. Briefly, primary cortical neurons were obtained from a pregnant ICR mouse at E18 (Charles River Laboratories, Wilmington MA). Briefly, mice were euthanized, and embryos were retrieved. Cortical tissue was dissected from the mouse embryos, removed meninges around the brain. Cortical rinds were placed in PBS and cut into small pieces, 0.5–1 mm in length. After collection, cortical tissue was resuspended in 20 U/mL papain (Worthington Biochemical Corp., Lakewood NJ) and 1 mg/mL DNAse I (Worthington Biochemical Corp., Lakewood NJ) in DMEM/F12 (Thermo Fisher Scientific, Waltham MA). Tissue was digested at 37°C for 3–5 minutes, with occasional gentle trituration. Enzyme was neutralized in DMEM/F12 containing 0.5% v/v FBS (Thermo Fisher Scientific, Waltham MA) and cells were collected by centrifugation at 1000 rpm for 3 minutes. Cells were then seeded (density) and maintained for 3 days in DMEM/F12 containing N-2 and B-27 supplement (Thermo Fisher Scientific, Waltham MA) and 0.5% v/v FBS. All experimental procedures were approved by the Baylor College of Medicine Institutional Animal Care and use committee (IACUC) and performed according to the Animal Welfare Act and NIH guidelines for the care and use of animals.

2.2.3. Immunostaining and imaging—Cells were fixed with 4% paraformaldehyde for 10 min and rinsed with PBS. Permeabilization was performed with 0.3% Triton X in PBS and blocking with 10% Goat Serum in PBS for 1 hr. at room temperature. Cells were stained for neuronal marker, Tuj-1, Mouse anti-TUJ1 primary antibody (Biolegend, San

Diego CA), Goat anti-mouse IgG Alexa Fluor 488 (Invitrogen, Waltham MA) and DAPI as the counterstain (Table S2 and S3). Cells were imaged in a Zeiss Axio Imager M2m microscope using a 20x objective.

2.2.4. Sholl analysis for neuronal outgrowth—Four different experiments were performed, which included six images per group. In total, 24 images per group were analyzed with semi-automatic autopath neuron tracing using IMARIS (Oxford Instruments). Sholl analysis is a widely used method to quantify branch complexity in neurons [45,46]. Neurites and branches for each neuron in a field of view were traced and IMARIS was used to perform Sholl analysis, cell count, and dendrite count. Data analysis was performed following a blinding procedure as described in supporting information.

2.3. In vivo studies in a peripheral nerve crush injury

2.3.1. Sciatic Nerve crush Injury model—Primary sciatic nerve crush injury was performed as previously described [47,48]. In brief, 8–10-week old Female Sprague-Dawley rats (average weight 225 g) were purchased from Charles River Laboratories (Wilmington MA). Rats were anesthetized by isoflurane, hair from the left and right femur was clipped, and the area was cleaned and sterilized with betadine and 70% isopropyl alcohol swabs. The sciatic nerve was exposed by making a subcutaneous incision at the thigh and gently separating the intermuscular space. The nerve was crushed with fine forceps for 10s twice intercross. 1 μL of peptide hydrogel or control was injected into the injury site with a glass needle and an auto-nanoliter injector Nanoject II (Drummond Scientific, Broomall PA). For analysis of sciatic nerve cross-sections, the injury site was marked with a suture 5 mm distal from the crush injury. The muscle and skin were sutured separately, and animals were allowed to recover and monitored regularly during the course of the study. Animals were euthanized by asphyxiation while anesthetized at specific time points. The nerves were harvested and processed for histology. All experimental procedures were approved by the Baylor College of Medicine Institutional Animal Care and use committee (IACUC) and performed according to the Animal Welfare Act and NIH guidelines for the care and use of animals. The surgeon and experimental personnel followed a blinded procedure during the duration of the study, as is described in the supporting information.

2.3.2. Walking track analysis and Sciatic Function Index—The recovery of nerve function after injury was evaluated using a walking track and footprint analysis. At specific time points, the hind paws of the animals (n=4 per treatment) were stained with a dark dye and allowed to walk in a 5 × 32-inch walking track covered with white paper. The rat footprints were analyzed as shown in Figure 5a and the sciatic function index (SFI) was calculated with the following equation [49,50]:

$$\text{Sciatic Function Index} = -38.3\left(\text{PL}_{\text{Exp}} - \text{PL}_{\text{Ctrl}}\right)/\left(\text{PL}_{\text{Ctrl}}\right) + 109.5\left(\text{TS}_{\text{Exp}} - \text{TS}_{\text{Ctrl}}\right)/\left(\text{TS}_{\text{Ctrl}}\right) + 13.3\left(\text{ITS}_{\text{Exp}} - \text{ITS}_{\text{Ctrl}}\right)/\left(\text{ITS}_{\text{Ctrl}}\right) - 8.8$$

Where PL indicates the print length, TS represents the distance from the first to fifth toe, and ITS indicates the distance from the second to the fourth toe for an experimental ($_{exp}$) or control ($_{ctrl}$) foot. Four animals per group and three footprints per rat were measured from

the normal and experimental feet. Data analysis was performed following a blinding procedure as described in supporting information.

2.3.3. Histological Analysis

2.3.3.1. Tissue Processing and staining: Sciatic nerves (n=3 nerves per group) were fixed with 4% paraformaldehyde overnight at 4°C and processed for cryopreservation with 20% sucrose solution. Nerves were embedded in Optimal Cutting Temperature (OCT) compound (Sakura Finetek USA, Torrence CA) and frozen. Nerves were cut in 25 μm sections and processed for Hematoxylin & Eosin or fluorescent immunostaining using standard protocols. For immunostaining, sections were washed with PBS and permeabilized with 1% Triton-X overnight at room temperature. Tissue sections were rinsed and blocked for 1 hr. in 10% goat serum, then incubated overnight at 4°C with antibodies as indicated in Tables S2. After rinsing the primary antibody, sections were stained with the respective secondary antibodies (Table S3), DAPI and mounted using Vectashield antifade mounting medium (Vector laboratories, Burlingame CA). The tissue sections were imaged in a Zeiss Axio Imager M2m microscope. Data analysis was performed following a blinding procedure as described in supporting information.

2.3.4. Analysis of myelinated axons—Nerve cross-sections (n = 3 per group) were immunostained with mouse anti-TUJ1 (Biolegend, San Diego CA) and rabbit anti-MBP antibodies (Abcam) to visualize axons and myelin, respectively. Tile scans of sciatic nerve cross-sections were obtained using a Leica TCS SP8X laser confocal microscope (63X oil). The number of myelinated and unmyelinated axons were then counted using CellProfiler (www.cellprofiler.org) and ImageJ (imagej.nih.gov/ij/). Three nerves per group were analyzed and for each nerve, axons were counted in three different 100 × 100 μm representative areas. Data analysis was performed following a blinding procedure as described in supporting information.

2.3.5. Macrophage Quantification—Macrophages were quantified in the area immediately surrounding the hydrogel. Hydrogel areas were excluded from quantification and analysis due to autofluorescence and excessive clustering of cells. $CD68^+$ macrophages and $DAPI^+$ nuclei were counted semi-automatically using ImageJ particle analysis (imagej.nih.gov/ij/). Three nerves per group were analyzed, with images of at least 1,000 × 1,000 μm quantified per nerve. Data analysis was performed following a blinding procedure as described in supporting information.

2.4. Statistical analyses

Error bars represent standard error of the mean (SEM) unless otherwise stated. Differences between groups were determined using one-way ANOVA with Tukey's multiple comparisons test in GraphPad Prism v. 8.3.1. P-values <0.05 were considered significant.

3. Results and discussion

3.1. Biomimetic MDPs self-assemble into nanofibrous scaffolds

A panel of MDPs for nerve regeneration were designed by incorporating short neurite outgrowth-promoting peptide mimics to K_2 (Table 1). As described in previous work, MDPs such as K_2 generally self-assemble into antiparallel -sheet structures that form injectable hydrogels upon the addition of multivalent ions or ultrasonication [5,9,11,37,43]. After the addition of the mimetic peptide motifs, we examined the secondary structure, assembly, and rheological properties of the resulting materials. Circular dichroism (CD) and ATR-FTIR (Figure 2) confirmed that the addition of 4 to 11 residues do not substantially perturb the antiparallel -sheet structure. In CD, all peptides presented a minimum near 216 nm and a maximum near 198 nm, and IR peaks at 1695 cm^{-1} and near 1620 cm^{-1} which collectively are characteristic of this conformation [9,10].

Hydrogelation for most of the mimetic peptides, except K_2-IIKDI and O_5, was achieved by the addition of buffer containing phosphate ions (HBSS) into a 2% by weight peptide in 298 mM sucrose solution. For O_5, hydrogelation is induced by an ultrasonication treatment of a 1% by weight solution in 149 mM sucrose 0.5X HBSS. In the case of K_2-IIKDI, addition of ions to the peptide solution resulted in peptide aggregation and phase separation, likely due to the additional ion-complementary amino acids incorporated into the attached mimic sequence. Therefore, for K_2-IIKDI, hydrogelation was achieved by making a 2% by weight solution in 298 mM sucrose without buffer. In this condition, K_2-IIKDI forms a self-supporting hydrogel (Figure 2c–d and Figure S2) with a storage modulus (G') of 780 ± 115 Pa and a loss modulus (G") of 105 ± 22 Pa. These results confirm the hydrogel formation of K_2-IIKDI with the modified conditions, as evidenced by a highly dense nanofiber network observed in SEM (Figure 2d). K_2-IKVAV, K_2-KDI, and K_2-Ten-C form more compliant hydrogels at 1% by weight in 149 mM sucrose 0.5X HBSS with a G' of 229 ± 36, 215 ± 43, and 275 ± 74 Pa and G" of 26 ± 5, 17 ± 4, and 37 ± 16 Pa, respectively (Figure 2c). Despite the lower G' and G", these peptide materials retain a high-density network of nanofibers and form clear self-supporting hydrogels as well (Figure 2d and Figure S3). Additionally, all the functionalized K_2 peptides are thixotropic and can be easily syringe aspirated and injected, recovering at least 60% of their initial viscoelastic properties within 5 min after shear stress (Figure S2). This suggests that the modification of the simplest K_2 peptide sequence to include short mimetic peptide sequences only marginally altered the physical, viscoelastic properties, and hydrogelation conditions as compared to the K_2 MDP sequence alone. These properties are within the normal range for previously reported MDP hydrogels [5,10,18], and are not expected to significantly affect the biological activity of these materials.

3.2. Biomimetic MDPs promote neurite outgrowth *in vitro*

We first wanted to evaluate the potential of these MDPs to facilitate axonal regeneration through a rapid, facile screening method. One of the major goals for therapeutic strategies for peripheral nerve injury is to increase the rate of neurite outgrowth [51], and many screening assays use neurite outgrowth *in vitro* as a surrogate measure for neuronal process extension *in vivo* [52]. *In vitro* neurite outgrowth assays have been successfully used to

screen for genetic regulators of axon regeneration [53–55] as well as small molecules that enhance neuronal regeneration *in vivo* [56].

For this study, a primary neuron culture model was used to evaluate the bioactivity of MDPs to promote neurite outgrowth. Primary neurons were seeded onto glass coverslips coated with MDPs for various time course. The extent of neurite outgrowth was quantified and evaluated against outgrowth on poly-D-lysine (PDL) coated surfaces after 3 days in vitro. PDL-coated surfaces are commonly used in neurite growth assays using primary neuron cultures [57], thus serving as a suitable control. Cell morphology was visualized through staining neuronal cell bodies and processes, and branch complexity and number were compared through neurite tracing. These parameters are commonly used measures for quantifying neuronal outgrowth in vitro and have been used to identify regulators of axon regeneration [54,55].

After 3 days *in vitro*, increased neurite outgrowth was observed after seeding on most MDP-coated surfaces, as evidenced by highly branched morphologies compared to neurons cultured on the control substrate PDL (Figure 3a and Figure S4). K_2, K_2-IIKDI, K_2-IKVAV, and K_2-TenC all showed greater branch complexity, with an increase of at least 30% in mean branch number 15 μm from the soma (Figure 3a–b and Figure S4). Neurons seeded on K_2, K_2-IIKDI, K_2-IKVAV, and K_2-TenC-coated surfaces all had increases of more than 25% in the mean total number of dendrites per cell compared to PDL, with K_2-IIKDI having an increase of more than 45% (Figure 3c). On the other hand, the non-ionic MDP, O_5, led to significantly less branch complexity (Figure 3), while SLac, SLanc, and K_2-KDI did not show significant differences compared to control (Figure S4). Notably, all MDPs had equal or higher cellular attachment rates compared to PDL, except for the non-ionic MDP O_5, which had dramatically lower number of attached cells (Figure S5).

These results show that K_2 and most functionalized MDPs with ECM and growth factor motifs promote cell attachment and neurite outgrowth. K_2, K_2-IIKDI, K_2-IKVAV, and K_2-TenC led to the greatest increases in neurite outgrowth, based on both Sholl analysis and total dendrite counts. Interestingly, K_2-KDI did not promote neurite outgrowth to the same extent as K_2, suggesting that the addition of the bioactive mimic may have counteracted K_2's intrinsic bioactivity. Two other MDPs, SLac and SLanc, did not enhanced neurite outgrowth as well relative to PDL. These peptides have an enzymatic cleavage domain that accelerates their degradation compared to K_2 (Table 1), which may account for these differences in performance.

From in vitro screening, we identified four peptides (K_2, K_2-IIKDI, K_2-IKVAV, and K_2-TenC) that promoted significantly more neurite outgrowth in comparison to PDL. These cellular responses could facilitate axonal regeneration in an injured nerve. The other peptides, SLac, SLanc, and K_2-KDI, had a similar performance to the control. Therefore, we reduced the peptide library and only studied the efficacy of K_2, K_2-IIKDI, K_2-IKVAV, and K_2-TenC in vivo.

3.3. MDP hydrogels are biocompatible and degradable in the sciatic nerve environment

To test the bioactivity of the MDPs in vivo, we performed sciatic nerve crush injury, which is a widely used model to understand the regenerative response in the PNS and its relevance to human disease [58]. Crushing of the sciatic nerve damages all axons and myelin sheaths but preserves the epineurium and basal lamina, which facilitate regeneration. After nerve crush, 1 μl of hydrogel was directly administered into the epineurium through direct injection without the need of conduits or autografts (Figure 4a–b). This system allows for the examination of MDP hydrogels' bioactivity alone, as no other materials were required for treatment of the injury. Variations in hydrogel presentation such as implant location and apparent implant size are due to limitations in histological methods; factors such as nerve rotation, relative position, and tissue quality during tissue processing can account for these differences. However, measures were taken such as the use of high precision nanoinjectors and glass needles to ensure a consistent amount of hydrogel was injected into each nerve.

After nerve crush, MDP hydrogels were found to be compatible with the peripheral nerve environment as evidenced by their degradation over time and the lack of abnormal nerve swelling over 21 days (Figure 4c, Figures S6–S7). High levels of growth cone-associated protein 43 (GAP-43), an indicator of axonal regrowth, shortly after crush injury demonstrates that the presence of the gels was not inhibitory to the acute regenerative response (Figure 4d, Figure S9). All K_2-based MDP hydrogels exhibited high levels of cellular infiltration, in contrast to O_5, where low infiltration was observed (Figure S8). Notably, Matrigel had neither cellular infiltration inside the hydrogel nor significant degradation over the same 21-day period (Figure S7–S8). The K_2 hydrogel has previously been demonstrated to elicit high macrophage infiltration in subcutaneous tissue [16,18], suggesting that this activity is also present in the peripheral nerve environment. Macrophage infiltration is known to be necessary for Wallerian degeneration, suggesting that K_2-based hydrogels may be beneficial to the early injury response. Together, these observations demonstrate that MDP hydrogels degrade in the peripheral nerve environment, do not adversely impact the early regenerative response, and may enhance immune cell recruitment after injury.

3.4. MDP Hydrogels accelerate functional recovery after sciatic nerve injury

After validating the hydrogel delivery method into the injury site, we then tested the MDPs for their capacity to promote functional recovery after crush injury. To measure functional recovery, we designed an experimental system based on the sciatic functional index (SFI). SFI is a reliable, sensitive, widely-used method of quantifying animal recovery after sciatic nerve injury that compares footprints from an injured side and an uninjured control side (Figure 5a) [49,59]. After severe sciatic nerve injury, footprints demonstrate an increase in print length and a decrease in toe spread and intermediate toe spread, owing to the loss of nerve and muscle function in the foot. As muscle reinnervation and myelin regeneration occur over time, proper muscle function is regained, leading to increasingly normal footprints (Figure 5b) [49,50,59].

Rats underwent sciatic nerve crush injury to one sciatic nerve, and MDP hydrogels were injected into the injury site immediately after crushing. The rats were placed on a walking

track 24 hours after surgery to collect footprints for SFI scoring. Walking track tests were performed periodically through 21 days post-injury. In our sciatic nerve crush injury system, we found that injured rats regained much of their sciatic nerve function by 21 days, leading to highly similar footprints from both injured and uninjured sides (Figure 5b and Figure S12). At 15 and 17 days post-injury rats treated with K_2, K_2-IIKDI, and K_2-IKVAV hydrogels had significantly higher SFI scores than rats whose nerves were injected with HBSS, Matrigel, O_5, SLac, and K_2-TenC (Figure 5c–e and Figure S10–S12). This shows that Matrigel, O_5, and SLac do not promote regeneration after sciatic nerve crush, and that addition of a Tenascin C motif to K_2 decreases its bioactivity. Overall, HBSS-treated rats regained approximately 80% of their original function in 21 days, as expressed by SFI score, while rats treated with K_2, K_2-IIKDI, and K_2-IKVAV reach the same degree of recovery four days earlier, an acceleration of healing of approximately 20%. This demonstrates that the MDP hydrogels K_2, K_2-IIKDI, and K_2-IKVAV promote accelerated functional recovery after sciatic nerve crush injury, suggesting that K_2 has intrinsic bioactivity in promoting the regenerative response, and the addition of laminin motifs IIKDI and IKVAV do not decrease its bioactivity.

3.5. MDP hydrogels facilitate accelerated myelination

After demonstrating that several MDPs promote functional recovery, we performed histological studies to understand the cellular responses that might account for this response. Previous studies have shown that the degree of axonal remyelination corresponds directly to the degree of functional recovery achieved after peripheral nerve injury [59,60]. In order to achieve efficient remyelination and functional recovery, injured nerves must first undergo Wallerian degeneration. We observed demyelination and the loss of axonal integrity as early as 3 days after crush injury, indicating that the MDP hydrogels allowed effective Wallerian degeneration (Figure S13–S14). To examine the extent of remyelination after hydrogel treatment, we obtained cross-sections of sciatic nerves treated with HBSS, Matrigel or MDP hydrogels at 15 days post-injury (Figure 6 and Figure S15), the time point at which differences in SFI were first observed (Figure 5c–e and Figure S13).

We observed an approximately 2-fold increase in the fraction of myelinated axons in nerves treated with the MDPs K_2, K_2-IIKDI, and K_2-IKVAV compared to the HBSS and Matrigel controls (Figure 6 and Figure S15). On the other hand, the fraction of myelinated axons in Matrigel, K_2-SLac, K_2-TenC, and O_5 were not significantly different from HBSS-treated control (Figure 6 and Figure S15). These results correlate with the extent of functional recovery as measured by SFI at the same time point (Figure 5 and Figures S10–S12), suggesting that K_2, K_2-IIKDI, and K_2-IKVAV facilitate accelerated myelination, leading to functional recovery.

3.6. MDP hydrogels recruit $CD68^+$ macrophages that may contribute to accelerated remyelination

The higher levels of remyelination observed after MDP hydrogel treatment may be attributed to an acceleration of the early degeneration response initiated by the nanofibrous hydrogels. Macrophages play a key role in Wallerian degeneration by clearing axon debris, assisting demyelination, secreting neurotrophic factors, and regulating Schwann cell maturation and

remyelination [27,61,62]. Indeed, depletion of macrophages in sciatic nerve crush injury has been shown to result in ineffective Wallerian degeneration and decreased functional recovery [63]. Given the previously demonstrated ability of K_2 to elicit an acute inflammatory response that resolves over time [18], we investigated whether an increase in macrophage infiltration could be observed which would suggest their mechanistic role.

In the sciatic nerve, all K_2-based MDPs presented rapid cellular infiltration upon injection (Figure 4 and Figures S6–S8) and were fully infiltrated by day 3. Through immunostaining, K_2 and functionalized MDP hydrogels were found to be highly infiltrated by $CD68^+$ macrophages at day 3 post-injury (Figure 7, outlines areas). On the other hand, HBSS-, O_5-, and Matrigel-treated nerves did not exhibit the same degree of macrophage recruitment (Figure 7 and Figures S16). As expected, more infiltrating macrophages were present in injured nerves compared with uninjured control (Figure S17). Early in the injury response at 3 days post-injury, K_2 and functionalized MDP hydrogels, K_2-IIKDI and K_2-IKVAV, were found to have more macrophages in the nerve areas around the implant (Figure 7a–b) and the hydrogels were highly infiltrated by macrophages. At 21 days post-injury, all injured nerves had a lower number of macrophages compared to the 3-day time point, as well as a higher number of $DAPI^+$ nuclei in the nerve area around the implant. No differences were found in the $CD68^+/DAPI^+$ ratios between any of the treated nerves and the HBSS-treated controls, suggesting that the acute macrophage response elicited by the MDP hydrogels did not lead to a long-lasting or chronic inflammatory response that could be inhibitory to nerve regeneration. The rapid recruitment of macrophages to the sites of MDPs administration may help account for the differences in myelination observed later in recovery, where K_2, K_2-IIKDI, and K_2-IKVAV have increased amounts of myelination compared with controls and other hydrogels (Figure 6). This increase in macrophage recruitment could then accelerate the degradation of axonal and myelin debris, creating a permissive environment for faster remyelination. Together, these results show that K_2-based MDP hydrogels promote recruitment of macrophages to the injury site and subsequent remyelination, resulting in accelerated functional recovery after peripheral nerve injury.

Other promising experimental strategies for peripheral nerve injury include growth factor administration [64,65], human- and animal-derived materials [41,66,67], and peptide-based hydrogels [68–71]. Differences in experimental variables such as rat strain and severity of injury lead to considerable variability between study results; as such, recovery times for crush injury studies can range from 21 days to 12 weeks to reach similar levels of functional recovery based on the SFI scoring system [41,66,68]. However, compared to other studies with similar injury severity, the administration of K_2-based MDP hydrogels alone led to functional recovery comparable to human keratin sponge conduits or direct NGF administration with collagen [64,66]. In contrast with other similar strategies, our system utilizes a simple single-component synthetic peptide hydrogel that accelerates nerve regeneration without the need of exogenous proteins, cells, and complex multi-component scaffolds. Together, our results demonstrate the potential for K_2-based MDPs as therapeutic materials for peripheral nerve regeneration. The inherent bioactivity and biocompatibility of K_2-based MDP hydrogels combined with their capacity for controlled release of therapeutic agents make them excellent platforms for developing improved strategies for nervous system regeneration [12,13].

4. Conclusion

Various self-assembling multidomain peptide (MDP) hydrogels were developed by adding short bioactive peptide motifs to a base peptide called K_2. The motifs are based on peptide mimics from ECM proteins known to have neurite outgrowth-promoting activity. The addition of these peptide motifs did not significantly alter self-assembly and nanofiber formation, and therefore the hydrogelation properties of these peptide materials. *In vitro* screening was performed through primary neuronal culture on MDP-coated glass coverslips to test peptide bioactivity for promoting neurite outgrowth. All lysine-based MDPs increased cell attachment and branching complexity of cultured neurons compared to PDL or the non-ionic MDP, O_5. From these *in vitro* experiments, K_2. K_2-IIKDI, K_2-IKVAV and K_2-TenC were observed to promote significantly more neurite outgrowth than PDL.

Sciatic nerve crush injury was used as a model for testing peptide hydrogel bioactivity to promote nerve regeneration and functional recovery. All peptide hydrogels are easily injectable into the injury site and degrade over time. The presence of these materials do not adversely affect nerve regeneration, as evidenced by uniform expression of GAP-43 across all hydrogel-treated nerves. Hydrogels are biocompatible, elicit high levels of cellular infiltration, and are integrated into the nerve tissue. Animals treated with K_2, K_2-IIKDI, and K_2-IKVAV showed accelerated functional recovery in comparison with HBSS, Matrigel and the non-ionic MDP O_5. Animals treated with HBSS, O_5, SLac, and K_2-TenC required 21 days to regain approximately 80% of their original function, while animals treated with K_2, K_2-IIKDI, and K_2-IKVAV reached the same level of recovery four days earlier.

These differences in functional recovery may be attributed to increased macrophage infiltration post-injury and accelerated remyelination. K_2-based peptide hydrogels recruit more macrophages into the material and injury site, which may lead to faster axonal degeneration and clearance of myelin debris early in the injury response. Sciatic nerves treated with K_2, K_2-IIKDI, and K_2-IKVAV had approximately double the fraction of remyelinated axons, correlating with increased functional recovery. This work demonstrates that K_2 and K_2-based hydrogels are beneficial to peripheral nerve injury recovery and promote pro-regenerative responses from multiple cell types in the PNS. While this proof-of-concept study exhibits the potential use of these materials in peripheral nerve injury, the use of more challenging injury models and improved delivery methods will shed more light on its therapeutic applications. Given these limitations, the promising results from this study provide important insight into biomaterial design and application of MDP hydrogels for injuries both in the PNS and CNS.

Supplementary Material

Refer to Web version on PubMed Central for supplementary material.

Acknowledgments

This work was supported in part by funding from the NIH (DE021798) and the Welch Research Foundation (C1557). TLLS and VLA were supported by the Mexican National Council for Science and Technology (CONACyT) Ph.D. Scholarship Program (678341 and 862901). EL was supported by the NSF Graduate Research Fellowship Program under grant No. 1842494.

References

[1]. Christman KL, Regenerative medicine: Biomaterials for tissue repair, Science. 363 (2019) 340–341. 10.1126/science.aar2955. [PubMed: 30679357]

[2]. Li J, Mooney DJ, Designing hydrogels for controlled drug delivery, Nat. Rev. Mater 1 (2016) 16071 10.1038/natrevmats.2016.71. [PubMed: 29657852]

[3]. Altunbas A, Pochan DJ, Peptide-Based and Polypeptide-Based Hydrogels for Drug Delivery and Tissue Engineering, in: Deming TJ (Ed.), Pept. Mater, Springer-Verlag Berlin Heidelberg, 2012: pp. 135–168. 10.1007/128_2011_206.

[4]. Hosoyama K, Lazurko C, Muñoz M, McTiernan CD, Alarcon EI, Peptide-based functional biomaterials for soft-tissue repair, Front. Bioeng. Biotechnol 7 (2019). 10.3389/fbioe.2019.00205.

[5]. Moore AN, Hartgerink JD, Self-Assembling Multidomain Peptide Nanofibers for Delivery of Bioactive Molecules and Tissue Regeneration, Acc. Chem. Res 50 (2017) 714–722. 10.1021/acs.accounts.6b00553. [PubMed: 28191928]

[6]. Mehrban N, Zhu B, Tamagnini F, Young FI, Wasmuth A, Hudson KL, Thomson AR, Birchall MA, Randall AD, Song B, Woolfson DN, Functionalized α-Helical Peptide Hydrogels for Neural Tissue Engineering, ACS Biomater. Sci. Eng 1 (2015) 431–439. 10.1021/acsbiomaterials.5b00051. [PubMed: 26240838]

[7]. Black KA, Lin BF, Wonder EA, Desai SS, Chung EJ, Ulery BD, Katari RS, Tirrell MV, Biocompatibility and Characterization of a Peptide Amphiphile Hydrogel for Applications in Peripheral Nerve Regeneration, Tissue Eng. Part A 21 (2015) 1333–1342. 10.1089/ten.tea.2014.0297. [PubMed: 25626921]

[8]. Marchini A, Raspa A, Pugliese R, Abd El Malek M, Pastori V, Lecchi M, Vescovi AL, Gelain F, Multifunctionalized hydrogels foster hNSC maturation in 3D cultures and neural regeneration in spinal cord injuries, Proc. Natl. Acad. Sci. U. S. A 116 (2019) 7483–7492. 10.1073/pnas.1818392116. [PubMed: 30923117]

[9]. Dong H, Paramonov SE, Aulisa L, Bakota EL, Hartgerink JD, Self-assembly of multidomain peptides: Balancing molecular frustration controls conformation and nanostructure, J. Am. Chem. Soc 129 (2007) 12468–12472. 10.1021/ja072536r. [PubMed: 17894489]

[10]. Aulisa L, Dong H, Hartgerink JD, Self-assembly of multidomain peptides: Sequence variation allows control over cross-linking and viscoelasticity, Biomacromolecules. 10 (2009) 2694–2698. 10.1021/bm900634x. [PubMed: 19705838]

[11]. Lopez-Silva TL, Leach DG, Li I-CI, Wang X, Hartgerink JD, Self-Assembling Multidomain Peptides: Design and Characterization of Neutral Peptide-Based Materials with pH and Ionic Strength Independent Self-Assembly, ACS Biomater. Sci. Eng 5 (2018) 977–985. 10.1021/acsbiomaterials.8b01348. [PubMed: 31404449]

[12]. Li IC, Moore AN, Hartgerink JD, “Missing Tooth” Multidomain Peptide Nanofibers for Delivery of Small Molecule Drugs, Biomacromolecules. 17 (2016) 2087–2095. 10.1021/acs.biomac.6b00309. [PubMed: 27253735]

[13]. Leach DG, Dharmaraj N, Piotrowski SL, Lopez-Silva TL, Lei YL, Sikora AG, Young S, Hartgerink JD, STINGel: Controlled release of a cyclic dinucleotide for enhanced cancer immunotherapy, Biomaterials. 163 (2018) 67–75. 10.1016/j.biomaterials.2018.01.035. [PubMed: 29454236]

[14]. Bakota EL, Wang Y, Danesh FR, Hartgerink JD, Injectable multidomain peptide nanofiber hydrogel as a delivery agent for stem cell secretome, Biomacromolecules. 12 (2011) 1651–1657. 10.1021/bm200035r. [PubMed: 21417437]

[15]. Roeckl-Wiedmann I, Bennett M, Kranke P, Systematic review of hyperbaric oxygen in the management of chronic wounds, Br. J. Surg 92 (2005) 24–32. 10.1002/bjs.4863. [PubMed: 15635604]

[16]. Carrejo NC, Moore AN, Lopez Silva TL, Leach DG, Li I-C, Walker DR, Hartgerink JD, Multidomain Peptide Hydrogel Accelerates Healing of Full-Thickness Wounds in Diabetic Mice, ACS Biomater. Sci. Eng 4 (2018) 1386–1396. 10.1021/acsbiomaterials.8b00031. [PubMed: 29687080]

[17]. Moore AN, Lopez Silva TL, Carrejo NC, Origel Marmolejo CA, Li I-C, Hartgerink JD, Nanofibrous peptide hydrogel elicits angiogenesis and neurogenesis without drugs, proteins, or cells, Biomaterials. 161 (2018) 154–163. 10.1016/j.biomaterials.2018.01.033. [PubMed: 29421552]

[18]. Lopez-Silva TL, Leach DG, Azares A, Li I-C, Woodside DG, Hartgerink JD, Chemical functionality of multidomain peptide hydrogels governs early host immune response, Biomaterials. 231 (2020). 10.1016/j.biomaterials.2019.119667.

[19]. Pfister BJ, Gordon T, Loverde JR, Kochar AS, Mackinnon SE, Kacy Cullen D, Biomedical engineering strategies for peripheral nerve repair: Surgical applications, state of the art, and future challenges, Crit. Rev. Biomed. Eng 39 (2011) 81–124. 10.1615/CritRevBiomedEng.v39.i2.20. [PubMed: 21488817]

[20]. Belin S, Zuloaga KL, Poitelon Y, Influence of mechanical stimuli on schwann cell biology, Front. Cell. Neurosci 11 (2017) 347 10.3389/fncel.2017.00347. [PubMed: 29209171]

[21]. George EB, Glass JD, Griffin JW, Axotomy-induced axonal degeneration is mediated by calcium influx through ion-specific channels, J. Neurosci 15 (1995) 6445–6452. 10.1523/jneurosci.15-10-06445.1995. [PubMed: 7472407]

[22]. Sievers C, Platt N, Perry VH, Coleman MP, Conforti L, Neurites undergoing Wallerian degeneration show an apoptotic-like process with annexin V positive staining and loss of mitochondrial membrane potential, Neurosci. Res 46 (2003) 161–169. 10.1016/S0168-0102(03)00039-7. [PubMed: 12767479]

[23]. Holtzman E, Novikoff AB, Lysomes in the rat sciatic nerve following crush., J. Cell Biol 27 (1965) 651–669. 10.1083/jcb.27.3.651. [PubMed: 5885432]

[24]. Lee HK, Shin YK, Jung J, Seo SY, Baek SY, Park HT, Proteasome inhibition suppresses schwann cell dedifferentiation in vitro and in vivo, Glia. 57 (2009) 1825–1834. 10.1002/glia.20894. [PubMed: 19455715]

[25]. Meyer Zu Hörste G, Hu W, Hartung H-P, Lehmann HC, Kieseier BC, The immunocompetence of Schwann cells, Muscle Nerve. 37 (2008) 3–13. 10.1002/mus.20893. [PubMed: 17823955]

[26]. Hirata K, Mitoma H, Ueno N, He JW, Kawabuchi M, Differential response of macrophage subpopulations to myelin degradation in the injured rat sciatic nerve., J. Neurocytol 28 (1999) 685–95. 10.1023/a:1007012916530. [PubMed: 10851347]

[27]. Gaudet AD, Popovich PG, Ramer MS, Wallerian degeneration: gaining perspective on inflammatory events after peripheral nerve injury, J. Neuroinflammation 8 (2011) 110 10.1186/1742-2094-8-110. [PubMed: 21878126]

[28]. Chen Z-L, Yu W-M, Strickland S, Peripheral Regeneration, Annu. Rev. Neurosci 30 (2007) 209–233. 10.1146/annurev.neuro.30.051606.094337. [PubMed: 17341159]

[29]. Makwana M, Raivich G, Molecular mechanisms in successful peripheral regeneration, FEBS J. 272 (2005) 2628–2638. 10.1111/j.1742-4658.2005.04699.x. [PubMed: 15943798]

[30]. Chen ZL, Strickland S, Laminin 1 is critical for Schwann cell differentiation, axon myelination, and regeneration in the peripheral nerve, J. Cell Biol 163 (2003) 889–899. 10.1083/jcb.200307068. [PubMed: 14638863]

[31]. Tashiro K, Sephel GC, Weeks B, Sasaki M, Martin GR, Kleinman HK, Yamada Y, A synthetic peptide containing the IKVAV sequence from the A chain of laminin mediates cell attachment, migration, and neurite outgrowth, J. Biol. Chem 264 (1989) 16174–16182. https://doi.org/VL - 264. [PubMed: 2777785]

[32]. Liebkind R, Laatikainen T, Liesi P, Is the soluble KDI domain of gamma1 laminin a regeneration factor for the mammalian central nervous system?, J. Neurosci. Res 73 (2003) 637–43. 10.1002/jnr.10692. [PubMed: 12929131]

[33]. Liesi P, Laatikainen T, Wright JM, Biologically active sequence (KDI) mediates the neurite outgrowth function of the gamma-1 chain of laminin-1, J. Neurosci. Res 66 (2001) 1047–1053. 10.1002/jnr.1250. [PubMed: 11746436]

[34]. Liesi P, Närvänen A, Soos J, Sariola H, Snounou G, Identification of a neurite outgrowth-promoting domain of laminin using synthetic peptides., FEBS Lett. 244 (1989) 141–148. 10.1016/0014-5793(89)81474-7. [PubMed: 2924902]

[35]. Faissneg A, Gttz B, Joester A, Scholze A, The tenascin gene family versatile glycoproteins implicated in neural pattern formation and regeneration, Semin. Dev. Biol 6 (1995) 139–148.

[36]. Midwood KS, Hussenet T, Langlois B, Orend G, Advances in tenascin-C biology, Cell. Mol. Life Sci 68 (2011) 3175–3199. 10.1007/s00018-011-0783-6. [PubMed: 21818551]

[37]. Kumar VA, Taylor NL, Shi S, Wang BK, Jalan AA, Kang MK, Wickremasinghe NC, Hartgerink JD, Highly angiogenic peptide nanofibers., ACS Nano. 9 (2015) 860–868. 10.1021/nn506544b. [PubMed: 25584521]

[38]. Meiners S, Nur-e-Kamal MS, Mercado ML, Identification of a neurite outgrowth-promoting motif within the alternatively spliced region of human tenascin-C., J. Neurosci 21 (2001) 7215–25. https://doi.org/21/18/7215 [pii]. [PubMed: 11549732]

[39]. Mercado MLT, Neurite Outgrowth by the Alternatively Spliced Region of Human Tenascin-C Is Mediated by Neuronal a7b1 Integrin, J. Neurosci 24 (2004) 238–247. 10.1523/JNEUROSCI.4519-03.2004. [PubMed: 14715956]

[40]. Timmer M, Robben S, Müller-Ostermeyer F, Nikkhah G, Grothe C, Axonal regeneration across long gaps in silicone chambers filled with Schwann cells overexpressing high molecular weight FGF-2, Cell Transplant. 12 (2003) 265–277. 10.3727/000000003108746821. [PubMed: 12797381]

[41]. Zou JL, Liu S, Sun JH, Yang WH, Xu YW, Rao ZL, Jiang B, Zhu QT, Liu XL, Wu JL, Chang C, Mao HQ, Ling EA, Quan DP, Zeng YS, Peripheral Nerve-Derived Matrix Hydrogel Promotes Remyelination and Inhibits Synapse Formation, Adv. Funct. Mater 28 (2018) 1–12. 10.1002/adfm.201705739.

[42]. Huang CW, Hsueh YY, Huang WC, Patel S, Li S, Multipotent vascular stem cells contribute to neurovascular regeneration of peripheral nerve, Stem Cell Res. Ther 10 (2019) 1–9. 10.1186/s13287-019-1317-7. [PubMed: 30606242]

[43]. Galler KM, Aulisa L, Regan KR, D'Souza RN, Hartgerink JD, Self-assembling multidomain peptide hydrogels: Designed susceptibility to enzymatic cleavage allows enhanced cell migration and spreading, J. Am. Chem. Soc 132 (2010) 3217–3223. 10.1021/ja910481t. [PubMed: 20158218]

[44]. Hilgenberg LGW, Smith MA, Preparation of dissociated mouse cortical neuron cultures, J. Vis. Exp (2007). 10.3791/562.

[45]. Sholl D, Dendritic organization in the neurons of the visual and motor cortices of the cat., J. Anat 87 (1953) 387–406. [PubMed: 13117757]

[46]. Binley KE, Ng WS, Tribble JR, Song B, Morgan JE, Sholl analysis: A quantitative comparison of semi-automated methods, J. Neurosci. Methods 225 (2014) 65–70. 10.1016/j.jneumeth.2014.01.017. [PubMed: 24485871]

[47]. Pan YA, Misgeld T, Lichtman JW, Sanes JR, Effects of Neurotoxic and Neuroprotective Agents on Peripheral Nerve Regeneration Assayed by Time-Lapse Imaging In Vivo, J. Neurosci 23 (2003) 11479–11488. 10.1523/jneurosci.23-36-11479.2003. [PubMed: 14673013]

[48]. Magill CK, Tong A, Kawamura D, Hayashi A, Hunter DA, Parsadanian A, Mackinnon SE, Myckatyn TM, Reinnervation of the tibialis anterior following sciatic nerve crush injury: A confocal microscopic study in transgenic mice, Exp. Neurol 207 (2007) 64–74. 10.1016/j.expneurol.2007.05.028. [PubMed: 17628540]

[49]. de Medinaceli L, Freed WJ, Wyatt RJ, An index of the functional condition of rat sciatic nerve based on measurements made from walking tracks, Exp. Neurol 77 (1982) 634–643. 10.1016/0014-4886(82)90234-5. [PubMed: 7117467]

[50]. Bain JR, Mackinnon SE, Hunter DA, Functional evaluation of complete sciatic, peroneal, and posterior tibial nerve lesions in the rat, Plast. Reconstr. Surg 83 (1989) 129–136. 10.1097/00006534-198901000-00024. [PubMed: 2909054]

[51]. Rayner MLD, Laranjeira S, Evans RE, Shipley RJ, Healy J, Phillips JB, Developing an In Vitro Model to Screen Drugs for Nerve Regeneration, Anat. Rec 301 (2018) 1628–1637. 10.1002/ar.23918.

[52]. Al-Ali H, Beckerman SR, Bixby JL, Lemmon VP, In vitro models of axon regeneration, Exp. Neurol 287 (2017) 423–434. 10.1016/j.expneurol.2016.01.020. [PubMed: 26826447]

[53]. Sivasankaran R, Pei J, Wang KC, Zhang YP, Shields CB, Xu XM, He Z, PKC mediates inhibitory effects of myelin and chondroitin sulfate proteoglycans on axonal regeneration, Nat. Neurosci 7 (2004) 261–268. 10.1038/nn1193. [PubMed: 14770187]

[54]. Moore DL, Blackmore MG, Hu Y, Kaestner KH, Bixby JL, Lemmon VP, Goldberg JL, KLF family members regulate intrinsic axon regeneration ability, Science. 326 (2009) 298–301. 10.1126/science.1175737. [PubMed: 19815778]

[55]. Blackmore MG, Moore DL, Smith RP, Goldberg JL, Bixby JL, Lemmon VP, High content screening of cortical neurons identifies novel regulators of axon growth, Mol. Cell. Neurosci 44 (2010) 43–54. 10.1016/j.mcn.2010.02.002. [PubMed: 20159039]

[56]. Al-Ali H, Lee DH, Danzi MC, Nassif H, Gautam P, Wennerberg K, Zuercher B, Drewry DH, Lee JK, Lemmon VP, Bixby JL, Rational Polypharmacology: Systematically Identifying and Engaging Multiple Drug Targets to Promote Axon Growth, ACS Chem. Biol 10 (2015) 1939–1951. 10.1021/acschembio.5b00289. [PubMed: 26056718]

[57]. Al-Ali H, Blackmore M, Bixby JL, Lemmon VP, High Content Screening with Primary Neurons, Eli Lilly & Company and the National Center for Advancing Translational Sciences, 2013.

[58]. Bauder AR, Ferguson TA, Reproducible mouse sciatic nerve crush and subsequent assessment of regeneration by whole mount muscle analysis, J. Vis. Exp (2012). 10.3791/3606.

[59]. Kanaya F, Firrell JC, Breidenbach WC, Sciatic function index, nerve conduction tests, muscle contraction, and axon morphometry as indicators of regeneration, Plast. Reconstr. Surg 98 (1996) 1264–1274. 10.1097/00006534-199612000-00023. [PubMed: 8942915]

[60]. Bélanger E, Henry FP, Vallée R, Randolph MA, Kochevar IE, Winograd JM, Lin CP, Côté D, In vivo evaluation of demyelination and remyelination in a nerve crush injury model, Biomed. Opt. Express 2 (2011) 2698 10.1364/boe.2.002698. [PubMed: 22091449]

[61]. Benowitz LI, Popovich PG, Inflammation and axon regeneration, Curr. Opin. Neurol 24 (2011) 577–583. 10.1097/WCO.0b013e32834c208d. [PubMed: 21968547]

[62]. Stratton JA, Holmes A, Rosin NL, Sinha S, Vohra M, Burma NE, Trang T, Midha R, Biernaskie J, Macrophages Regulate Schwann Cell Maturation after Nerve Injury, Cell Rep 24 (2018) 2561–2572.e6. 10.1016/j.celrep.2018.08.004. [PubMed: 30184491]

[63]. Barrette B, Hébert MA, Filali M, Lafortune K, Vallières N, Gowing G, Julien JP, Lacroix S, Requirement of myeloid cells for axon regeneration, J. Neurosci 28 (2008) 9363–9376. 10.1523/JNEUROSCI.1447-08.2008. [PubMed: 18799670]

[64]. Sun W, Sun C, Lin H, Zhao H, Wang J, Ma H, Chen B, Xiao Z, Dai J, The effect of collagen-binding NGF-β on the promotion of sciatic nerve regeneration in a rat sciatic nerve crush injury model, Biomaterials. 30 (2009) 4649–4656. 10.1016/j.biomaterials.2009.05.037. [PubMed: 19573907]

[65]. Hong MH, Hong HJ, Pang H, Lee HJ, Yi S, Koh WG, Controlled Release of Growth Factors from Multilayered Fibrous Scaffold for Functional Recoveries in Crushed Sciatic Nerve, ACS Biomater. Sci. Eng 4 (2018) 576–586. 10.1021/acsbiomaterials.7b00801.

[66]. Gao J, Zhang L, Wei Y, Chen T, Ji X, Ye K, Yu J, Tang B, Sun X, Hu J, Human hair keratins promote the regeneration of peripheral nerves in a rat sciatic nerve crush model, J. Mater. Sci. Mater. Med 30 (2019) 1–13. 10.1007/s10856-019-6283-1.

[67]. Pace LA, Plate JF, Smith TL, Van Dyke ME, The effect of human hair keratin hydrogel on early cellular response to sciatic nerve injury in a rat model, Biomaterials. 34 (2013) 5907–5914. 10.1016/j.biomaterials.2013.04.024. [PubMed: 23680369]

[68]. Li A, Hokugo A, Yalom A, Berns EJ, Stephanopoulos N, McClendon MT, Segovia LA, Spigelman I, Stupp SI, Jarrahy R, A bioengineered peripheral nerve construct using aligned peptide amphiphile nanofibers, Biomaterials. 35 (2014) 8780–8790. 10.1016/j.biomaterials.2014.06.049. [PubMed: 25064803]

[69]. Hsu R, Chen P, Fang J, Chen Y, Chang C, Lu Y, Hu S, Adaptable Microporous Hydrogels of Propagating NGF-Gradient by Injectable Building Blocks for Accelerated Axonal Outgrowth, Adv. Sci 6 (2019) 1900520 10.1002/advs.201900520.

[70]. Wu X, He L, Li W, Li H, Wong WM, Ramakrishna S, Wu W, Functional self-assembling peptide nanofiber hydrogel for peripheral nerve regeneration, Regen. Biomater 4 (2017) 21–30. 10.1093/rb/rbw034. [PubMed: 28149526]

[71]. Faroni A, Workman VL, Saiani A, Reid AJ, Self-Assembling Peptide Hydrogel Matrices Improve the Neurotrophic Potential of Human Adipose-Derived Stem Cells, Adv. Healthc. Mater 8 (2019) 1900410 10.1002/adhm.201900410.

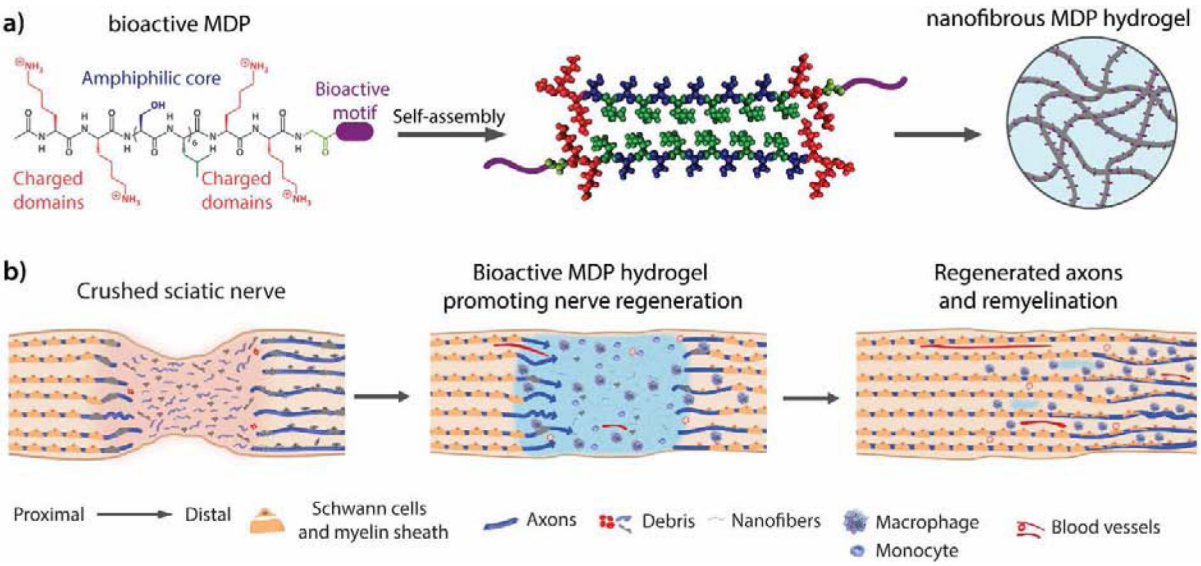

Figure 1.

Multidomain peptides for enhancing peripheral nerve regeneration. a) K_2-based MDPs bearing bioactive motifs derived from ECM proteins. b) After sciatic nerve crush injury, axons, myelin and ECM are damaged. Application of the K_2-based peptide hydrogels promote acute macrophage infiltration and accelerate axon growth and remyelination.

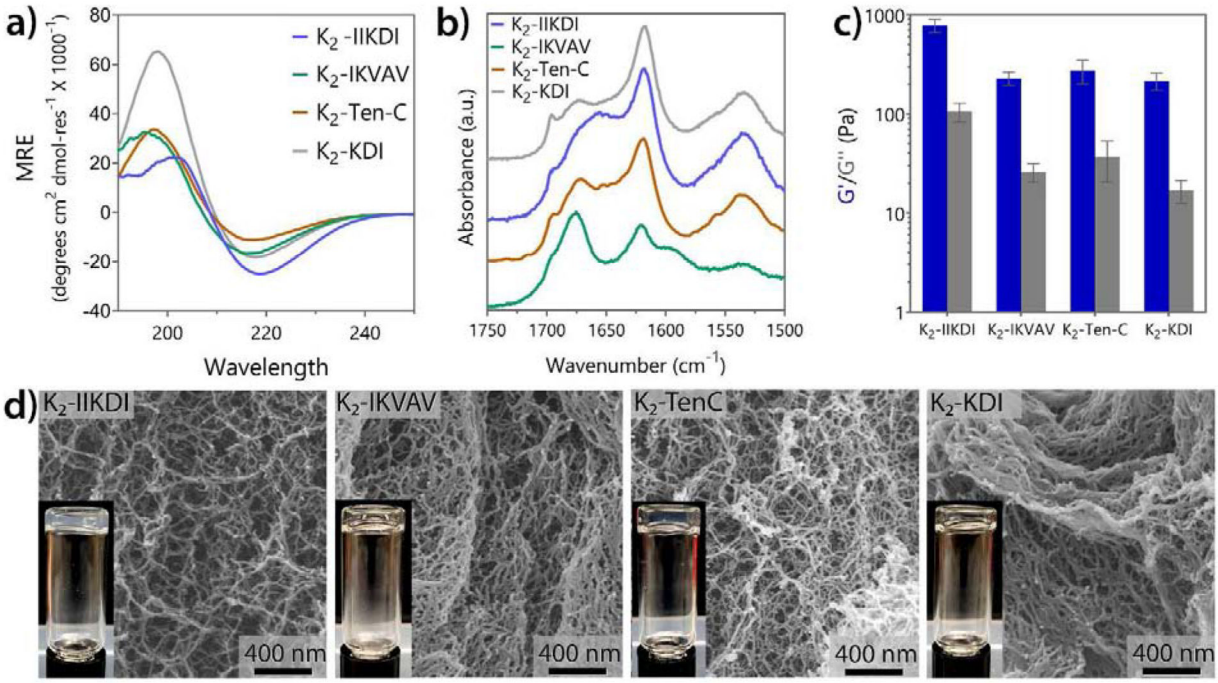

Figure 2.

K_2-based MDP functionalized with bioactive peptide mimics form nanofibrous soft materials. a) Circular dichroism spectroscopy of three K_2-based peptides containing laminin and Tenascin C peptide mimics. All peptides showed the characteristic spectrum of -sheet structure. b) ATR-FTIR spectra confirm all peptides are antiparallel -sheets. c) Storage and loss moduli of peptide hydrogels at 1% oscillatory strain (n = 3). Error bars represent standard deviation. d) SEM images of all MDPs hydrogels showing the nanofibrous network. Inserts show the self-supportive hydrogel material.

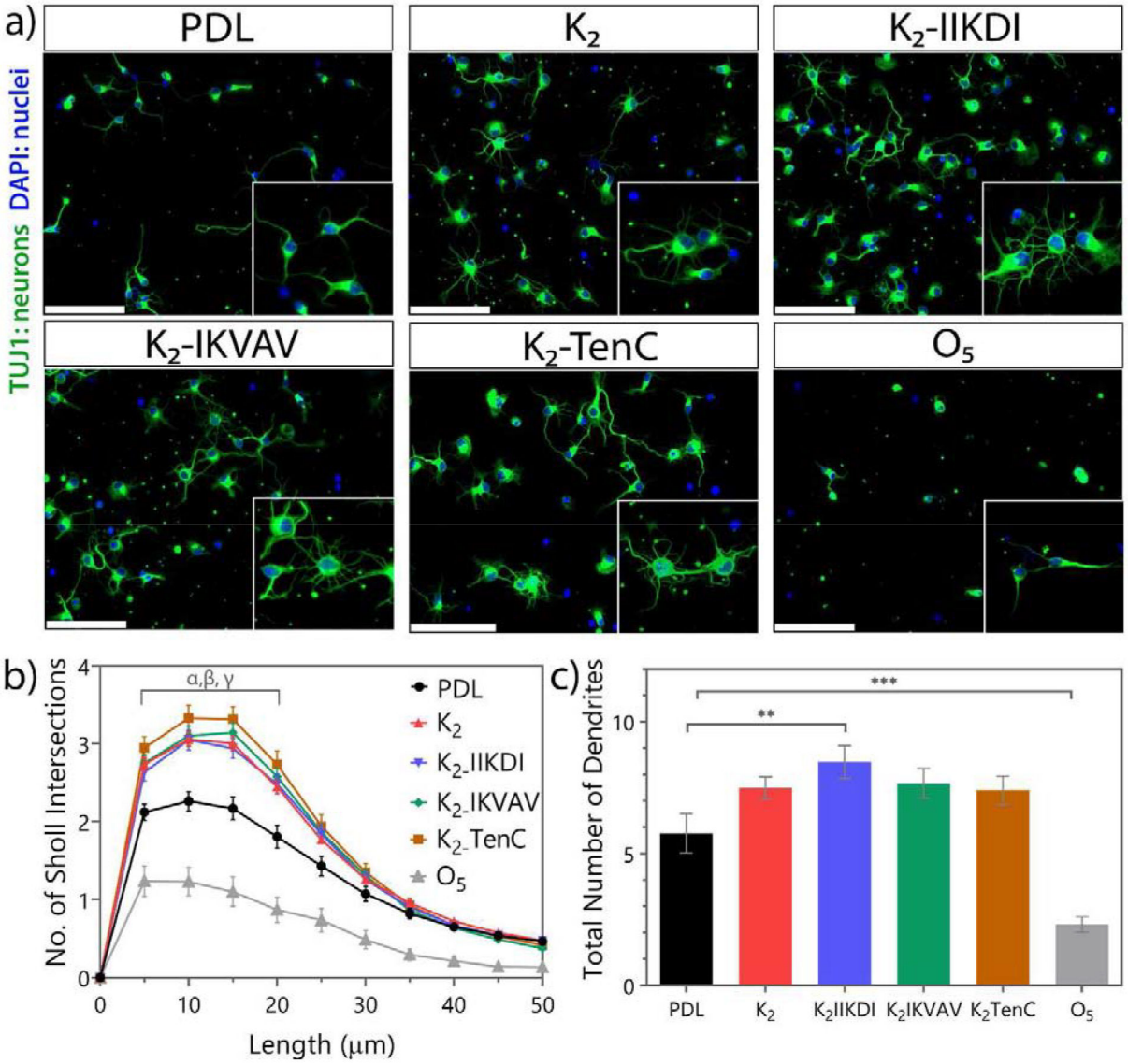

Figure 3.

Primary neuronal culture on peptide-coated coverslips shows differences in neuronal outgrowth. a) Representative images of cortical neurons three days of culture in peptide-coated glass. Scale bar 100 μm. b) Number of Sholl intersections at specific length. Sholl intersections from 5 to 20 μm of neurons cultured in MDPs are significantly different from PDL. α: K_2-IIKDI p-value < 0.05, α: K_2 and K_2-IKVAV p-value < 0.01, γ: K_2-TenC and O_5 (p-value 0.0001). c) Total number of dendrites per neuron. ** p-value < 0.01, *** p-value 0.0001. Error bars represent SEM n= 24 images from 4 separate experiments.

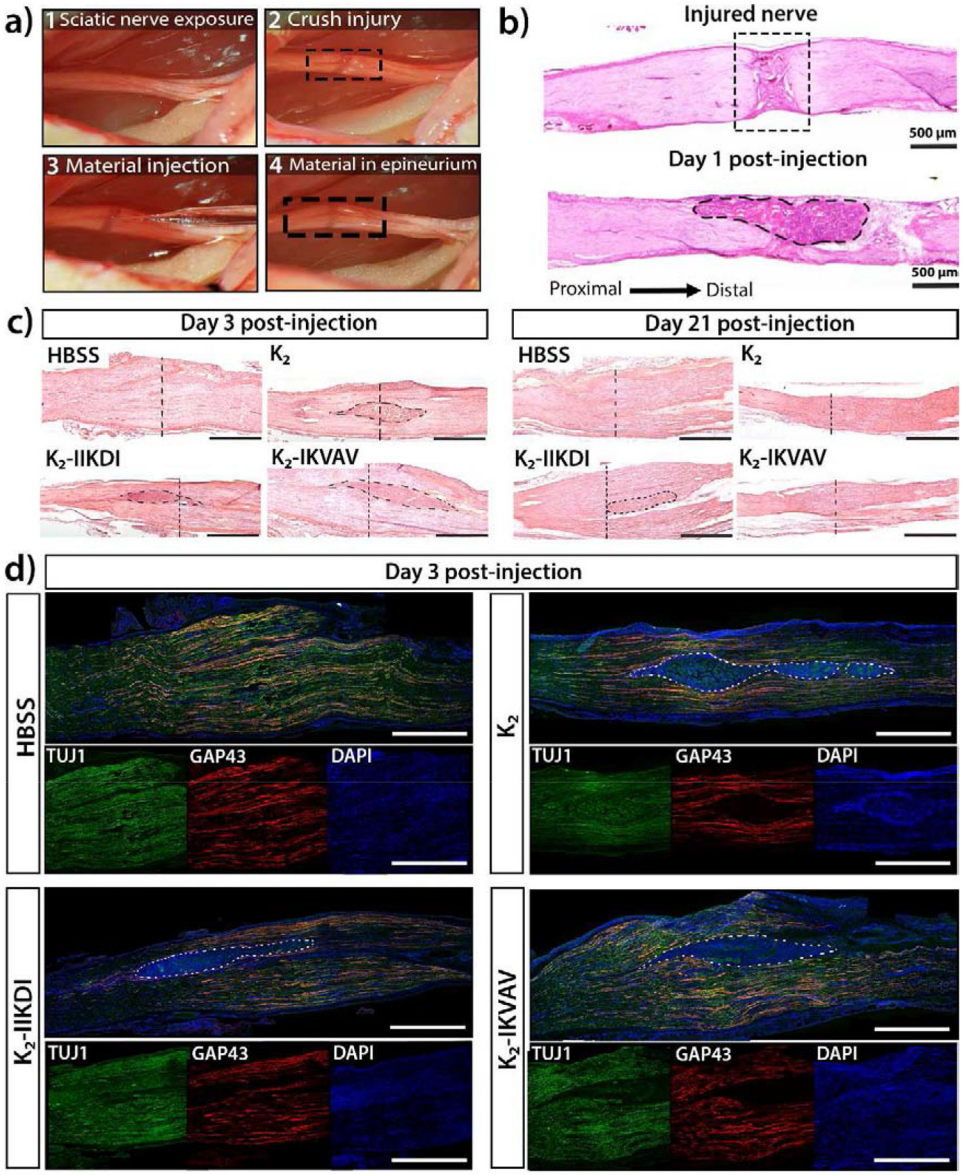

Figure 4.

Sciatic nerve crush injury model and hydrogel administration. a) The sciatic nerve was exposed and crushed, 1 μL of peptide hydrogel or control was injected directly into the injury site, using the epineurium to hold the material. b) H&E staining of an injured nerve showing the crush injury and axon disruption. Hydrogel is localized and held in place in the injury, as shown in the one-day post-injury tissue section. c) H&E staining of injured nerves treated with different materials three days and 21 days post-injury. Visible hydrogels are circled with a dotted line. A vertical dotted line indicates approximate center of crush injury. Scale bar is 1mm. d) Immunostaining for TUJ1 (axons), GAP43 (regenerating axons), and DAPI (cell nuclei) of sciatic nerves treated with HBSS, K_2, K_2-IIKDI, and K_2-IKVAV three days post injury. Visible hydrogels are circled with a dotted line, and high cellular infiltration can be observed in gels, as indicated by DAPI staining. Scale bar 1mm for merged and individual channel images.

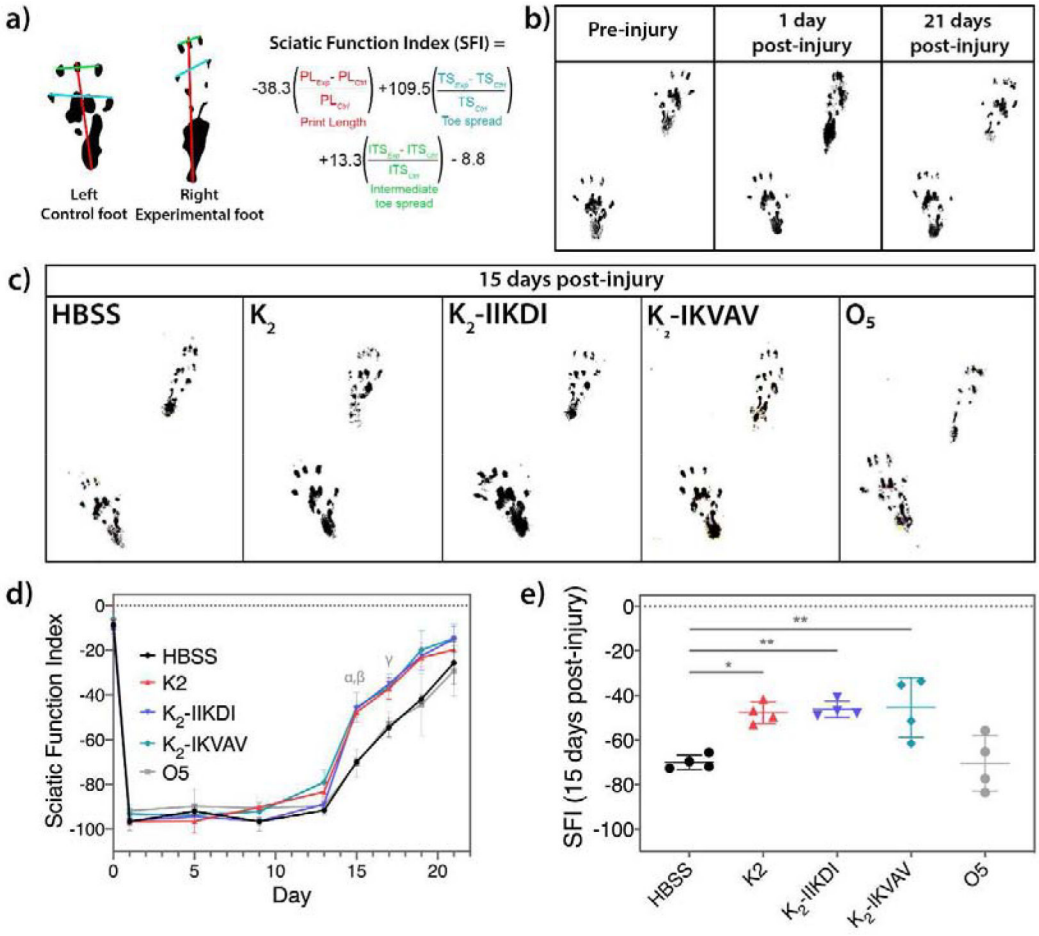

Figure 5.

MDPs accelerate functional recovery of sciatic nerve crush as observed in walking track analysis. a) Equation for calculating the Sciatic Function Index (SFI) using an uninjured control foot and the experimental foot. b) Footprints of rats pre-injury, one day post-injury, and 21 days post injury. c) Representative footprints of rats treated with HBSS control and MDP hydrogels. d) SFI scores from pre-injury to 21 days post-injury. Statistically significant differences compared with HBSS control are observed at 15 days post-injury (α: K_2 p-value <0.05, β: K_2-IIKDI and K_2-IIKDI p-value <0.01) and 17 days post-injury (γ: K_2, K_2-IIKDI and K_2-IKVAV p-value <0.01). e) Scatter plot with individual values representation of the SFI 15 days post-injury. Error bars represent standard deviation. n= 4 rats per group. * p-value < 0.05, ** p-value < 0.01.

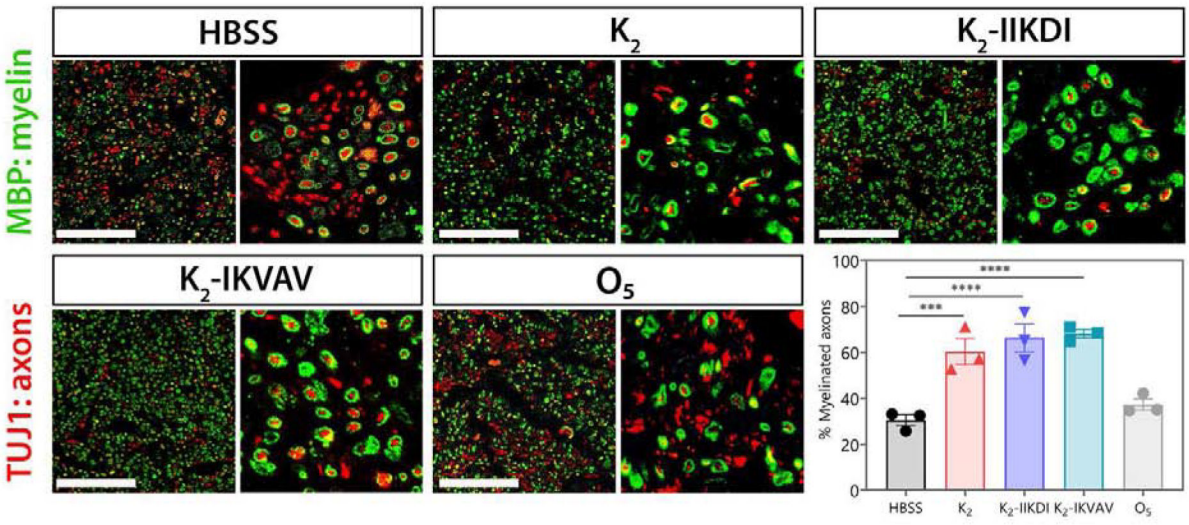

Figure 6.

Sciatic nerves show differential myelination after MDP hydrogel administration. Representative images of sciatic nerve cross-sections stained for TUJ1 (axons) and MBP (myelin) 15 days after crush injury. Cross sections are approximately 800 μm distal from the injury site. Scale bar 100 μm. The fraction of axons that are myelinated are significantly greater in nerves treated with K_2, K_2-IIKDI, and K_2-IKVAV compared to HBSS- or O_5-treated nerves. Error bars represent SEM. n = 3 animals per group,. **** p-value <0.0001, *** p-value < 0.0005.

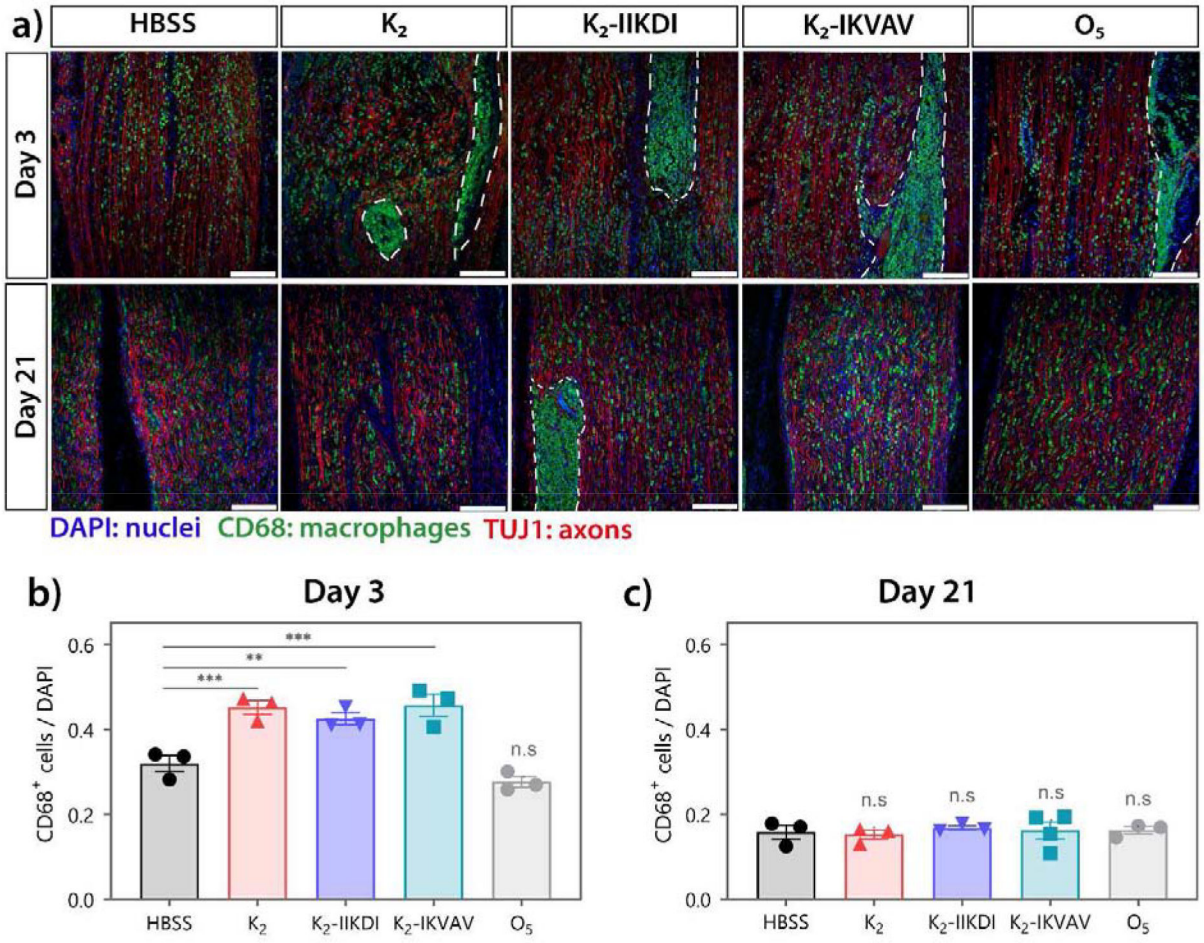

Figure 7.

High macrophage infiltration is observed in MDP treated nerves. CD68 and TUJ1 staining of sciatic nerves 3- and 21-days post-injury. a) Representative immunofluorescence images of injured sciatic nerves. Top panel: 3 days post-injury; bottom panel: 21 days post-injury. Dotted line: hydrogel. Scale bar 200 μm. b-c) Quantification of CD68+ macrophages relative to DAPI+ nuclei in areas surrounding hydrogel. Hydrogels were excluded in quantification due to autofluorescence and excessive clustering of cells. b) Nerves treated with K_2, K_2-IIKDI, and K_2-IKVAV had significantly greater $CD68^+/DAPI^+$ ratios compared to HBSS-injected control nerves. c) No significant differences were found in $CD68^+$/DAPI ratios between hydrogel-treated and HBSS-injected nerves. Error bars represent SEM. n= 3–4 animals per group. ** p-value < 0.01, *** p-value < 0.001

Table 1.

MDP sequences and their bioactive peptide mimics for promoting nerve regeneration

Name	Peptide sequence	Mimicking	Bioactivity
K_2 *	$K_2(SL)_6K_2$		
O_5 *	$(Hyp)_5(SL)_6(Hyp)_5$		
SLac *	$K(SL)_3RG(SL)_3K$**GRGDS**	enzyme cleavage	Cell attachment, degradable
SLanc *	$K(SL)_3RG(SL)_3K$**GKLTWQELYQLKYKGI**	VEGF	Degradable and angiogenic
K_2-IIKDI	$K_2(SL)_6K_2$**GRNIAEIIKDI**	Laminin γ1	Neurite outgrowth
K_2-IKVAV	$K_2(SL)_6K_2$**GIKVAV**	Laminin α1	Neurite outgrowth
K_2-TenC	$K_2(SL)_6K_2$**GVFDNFVLK**	Tenascin C	Neurite outgrowth
K_2-KDI	$K_2(SL)_6K_2$**GKDI**	Laminin γ1	Neurite outgrowth

* Previously published from References [10,11,37,43]